THE RISK TO SATELLITE TETHERS FROM METEOROID AND DEBRIS IMPACTS

Neil McBride and Emma A. Taylor

Unit for Space Sciences and Astrophysics
The Physics Laboratory, University of Kent, Canterbury, CT2 7NR, UK
Tel +44 (0)1227 823242, Fax +44 (0)1227 762616,Email N.McBride@ukc.ac.uk

ABSTRACT

This paper calculates the expected failure rate of typical single-chord tethers in Low Earth Orbit (LEO). We present a particulate flux model combined with an impact damage equation, which is tested for its applicability to tethers by light gas gun hypervelocity impact experiments. We find that long, thin (< 1 mm diameter) tethers are not viable for long duration missions. The model predicts the failure of the SEDS-2 tether (~20 km, ~0.75 mm) in under 2 weeks, consistent with what occurred. Thicker (and shorter) tethers are more viable; the model predicts that the TiPS tether (~4 km, ~2 mm) will have a lifetime of around 1 year.

1. INTRODUCTION

The use of satellite tethers will allow space applications such as power generation, low frequency antenna, deployment of instruments in the 100–200 km altitude region, and unfuelled orbital altitude changes of instruments. The deployment of such tethers has been demonstrated (though not without problems). However it is possible that impact failure from meteoroid or debris impact would seriously affect the viability of long duration tether missions. In order to deduce the risk to a tether strand due to hypervelocity impact, we consider the flux of potentially destructive particles in the orbital environment *i.e.* meteoroids and space debris, and then consider the hypervelocity impact response of typical tether materials.

2. PARTICULATE FLUX MODEL

We will start with the mass distribution of Grün *et al.* (1985) to model the meteoroid environment in LEO, and test the model against data from the Long Duration Exposure Facility (LDEF) which offers a large area-time product detector. The 'Grün flux' was derived from a variety of sources (meteor, lunar crater, and spacecraft data) and, while not assuming an isotropic meteoroid environment *per se*, the flux values were reduced to a mean exposure for a detector surface which was spinning. Therefore, when time averaged the *exposure* is pseudo-isotropic. The flux values themselves are given as cumulative annual mean values for a spinning flat plate detector 'at 1 AU', *i.e.* outside the gravitational influence of the Earth (but moving in an Earth-like orbit). However, if a detector has an essentially *randomised* viewing geometry then we can consider the flux model *itself* to be isotropic in nature, and integrate over all directions with regard to a flat plate detector (note for detectors orientated with respect to heliocentric space, this is not necessarily the case; see Taylor & McBride 1997).

Direct application of the flux values using a single mean velocity can be 'hazardous' since mean gravitational flux enhancement and Earth shielding factors are velocity dependent, and flux enhancement due to spacecraft motion (and overall exposure to spacecraft surfaces) is dependent on the orbital geometry as well as the meteoroid velocity distribution. Also the meteoroid damage capability is velocity dependent and so for failure analysis, a range of velocities should be used. We use a full meteoroid velocity distribution, in a model which takes account of instantaneous surface geometry and velocity dependent enhancements and Earth shielding considerations. The velocity distribution used (Fig. 1) originates from the Harvard Radio Meteor Project (HRMP) data (Southworth & Sekanina 1973; Sekanina & Southworth 1975) although it has been re-analysed by Taylor (1995a; 1995b) who corrected a coding error in the original distribution, which caused a gross under-estimation in the relative number of fast meteoroids.

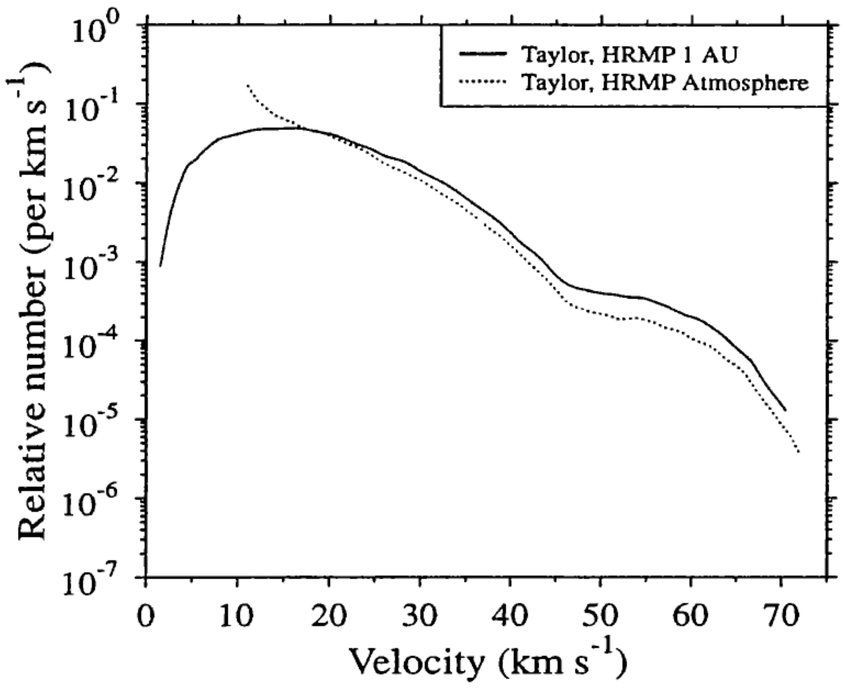

Figure 1: The amended HRMP meteoroid velocity distribution of Taylor (1995a; 1995b), converted to '1 AU'.

In the model, we use *differential* values of the Grün flux, F_G, and note that within the isotropic framework of the model, the flux *intensity* (number m^{-2} s^{-1} sr^{-1}) is F_G/π. We then consider the flux of particles encountered by a moving flat plate detector by integrating the flux intensity over all viewing angles, particle mass, and particle velocity. The total instantaneous flux contribution to the detector is then given by

$$F_m = \int_m \int_{v_\infty} \int_\phi \int_\theta \frac{F_G}{\pi} \, G \, n(v_\infty) \, \cos A \, \frac{v_{\mathrm{rel}}}{v_E} \sin\theta \; d\theta \; d\phi \; dv_\infty \; dm \qquad (1)$$

where θ, ϕ are spherical polar coordinates with the spacecraft at the origin, v_E is the gravitationally enhanced meteoroid velocity given by $\sqrt{v_\infty^2 + v_{\mathrm{esc}}^2}$ (where v_{esc} is the escape velocity at the spacecraft altitude), v_{rel} is the relative velocity of the incoming meteoroid with respect to the spacecraft *i.e.* v_{rel}/v_E accounts for the spacecraft moving through the meteoroid environment, and the angle A is the instantaneous impact angle to the face (measured from the face normal). G is the gravitational flux enhancement given by $1+(v_{\mathrm{esc}}^2/v_\infty^2)$ (using a realistic 'working range' for v_∞, of $1 < v_\infty < 72$ km s^{-1}). In numerical evaluation of Eq. 1, no instantaneous flux contribution is added if the meteoroid cannot impact the face (*i.e.* if $A > \pi/2$), or the spacecraft is shielded by the Earth.

2.1 Hypervelocity impact damage equation

For an instantaneous $d\theta$, $d\phi$, dV_∞ and dm step, a damage equation may be used to obtain the ballistic limit F_{max} (maximum thickness of a foil which would be just-perforated) of a spacecraft detector *i.e.* each flux contribution is binned at the appropriate F_{max} value for the θ, ϕ, v_∞, M element. We use the penetration '1992C' equation of McDonnell & Sullivan (1992):

$$\frac{F_{max}}{d_p} = 1.272 \, d_p^{0.056} \, V^{0.806} \times \left(\frac{\rho_p \rho_{\mathrm{Al}}}{\rho_{\mathrm{Fe}} \rho_t}\right)^{0.476} \left(\frac{\sigma_{\mathrm{Al}}}{\sigma_t}\right)^{0.134} \qquad (2)$$

where particle diameter d_p and F_{max} are in cm, and velocity V is in km s^{-1}. We use a meteoroid density of 2500 kg m^{-3} (as is used to derive the Grün flux).

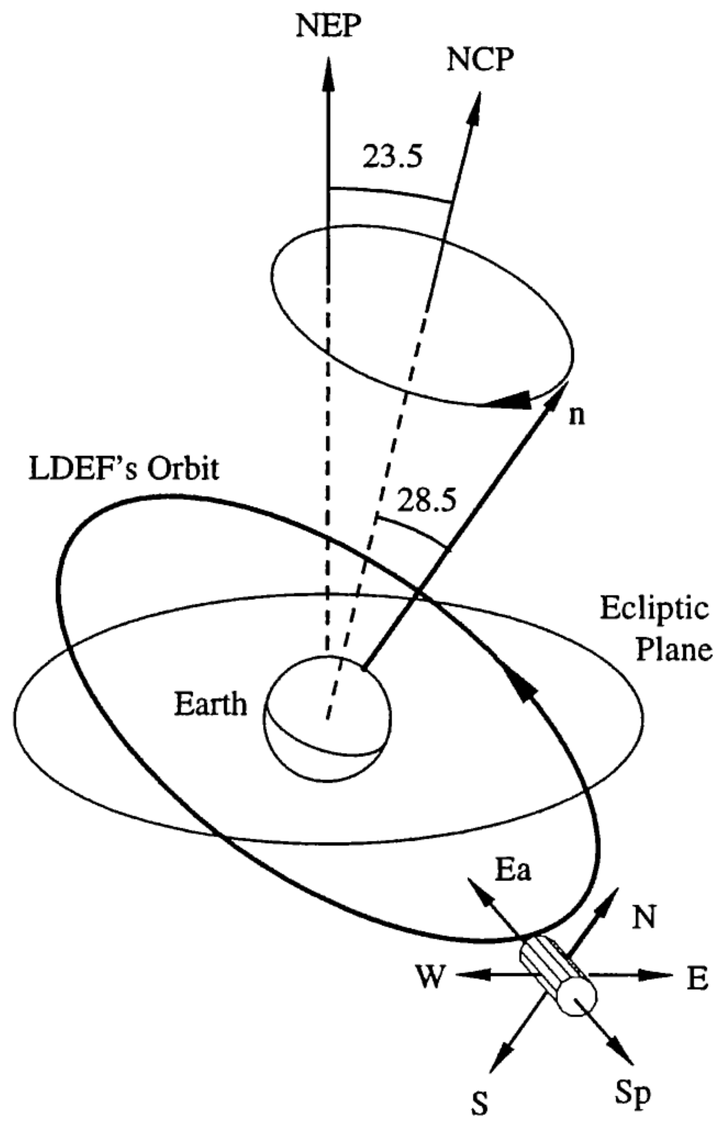

Figure 2: The orbit of LDEF. The orbit vector **n** precesses around the north celestial pole (NCP). The north ecliptic pole (NEP) is also shown. LDEF maintains its geometry with respect to Earth but is essentially randomised with respect to heliocentric space.

2.2 Application to LDEF

As a test we can apply the model to LDEF. Fig. 2 shows LDEF's gravity gradient stabilised orbit such that the faces maintained an orientation with respect

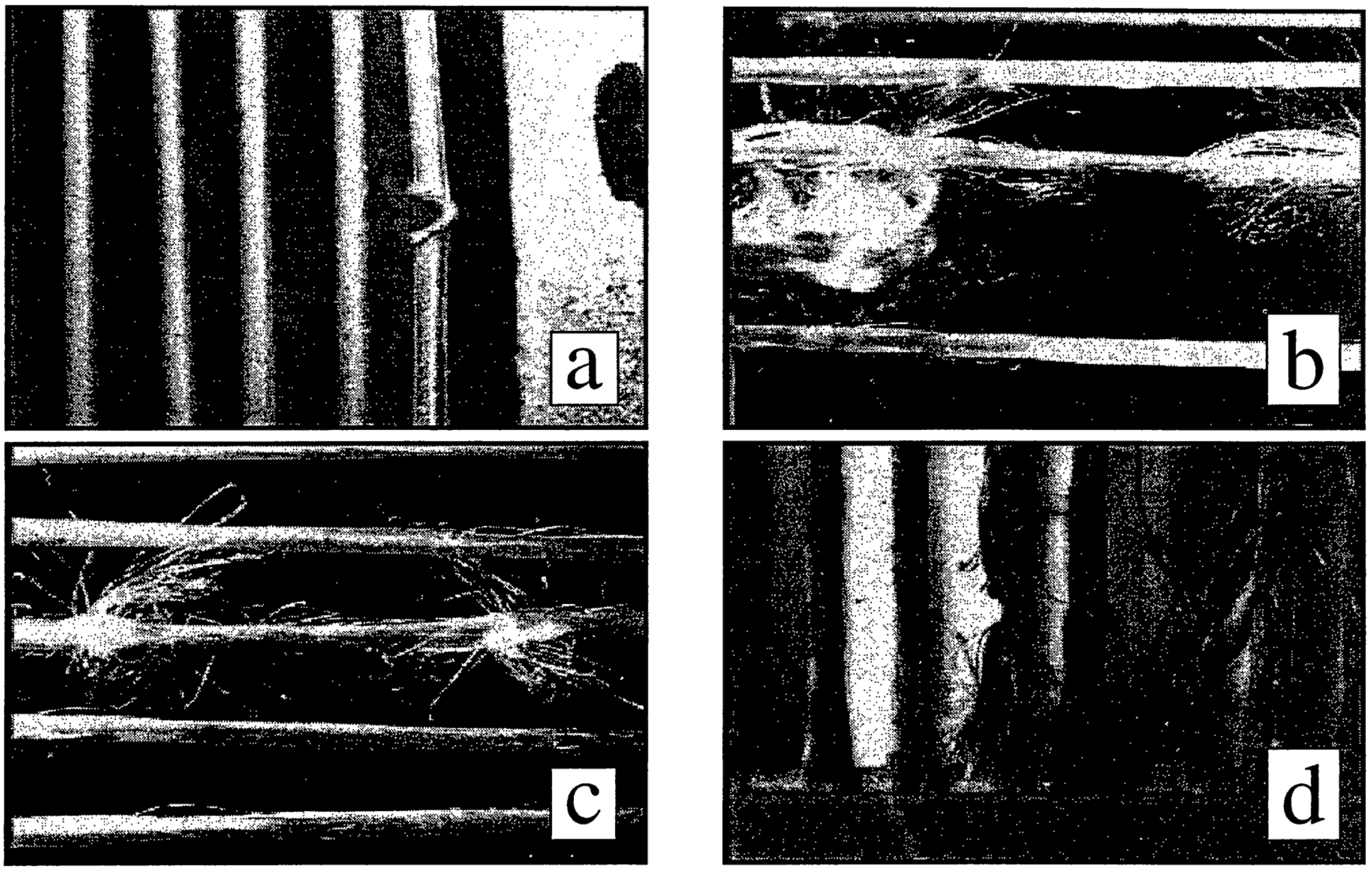

Figure 3: Impact tests at 5 km s^{-1}. (a) 300μm impactor on a 1 mm aluminium wire. The impact area has been turned through 90° for clarity. (b) 300μm impactor on Spectra 1000 0.75 mm tether. Note one strand completely broken and another damaged. (c) 200μm impactor on Spectra 1000 0.75 mm tether. No strands broken but considerable damaged seen. (d) 300μm impactors to Spectra 1000 0.75 mm tethers (not under tension). Note the 'bite' from a grazing impact, centre image.

to Earth (east, west, north, space etc). The orbit vector **n** precessed about the NCP with a period of ~52 days (see McBride *et al.* 1995 for a more detailed discussion). It is seen that the geometry of the space face with respect to heliocentric space, is essentially randomised over time (and with no Earth shielding), and so application of our isotropic meteoroid model is applicable to this case.

Fig. 4 shows the model applied to the space face of LDEF. For geometric reasons, very little orbital debris can impact the space face and so the space face offers an excellent *meteoroid* detector, and it is seen from Fig. 4 that the meteoroid model fits the space face data well. However, the other faces (north, south, east and west) contributing to the 5-face mean *do* encounter orbital debris. The dominance of debris in LEO is clearly seen at the smaller sizes ($F_{max} < 30\mu$m). However, at the larger size regime ($F_{max} > 30\mu$m) meteoroids are dominant (see McDonnell *et al.* 1997 for further analysis). It is this size regime (approaching mm) which is the most important for the consideration of catastrophic failure of tethers, since the meteoroids are large enough to cause tether failures, but numerous enough to offer significant risk within reasonable area-time products. For this reason, a consideration of tether risk can be performed by using the meteoroid model only.

3. APPLICATION OF MODEL TO TETHERS

Inspection of Fig. 2 shows that the exposure geometry of a LEO gravity stabilised tether is essentially identical to a (long, thin) LDEF-like cylinder, and so the model will be particularly appropriate in determining meteoroid fluxes to tethers. However, in applying the model in this way we must consider whether the foil penetration equation (Eq. 2) can be applied to a typical tether strand. Hence we must consider (1) the effect of a 'wire-like' cross section rather than a flat foil, (2) whether Eq. 2 adequately predicts the hypervelocity impact response of tether material, and what critical F_{max} would cause a failure of the tether strand, (3) target area effects. To assess these subjects, a hypervelocity impact

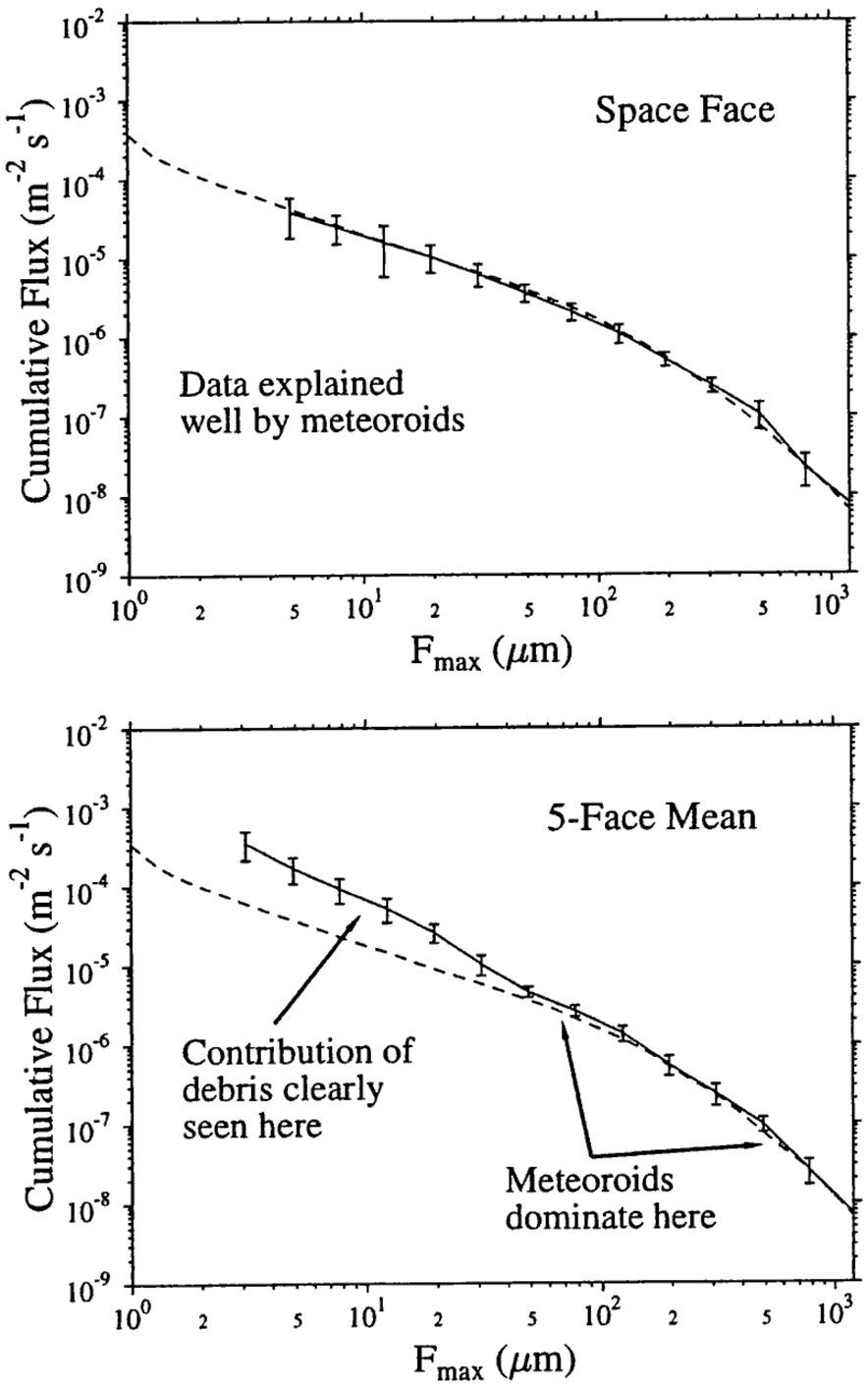

Figure 4: LDEF data is derived from a variety of sources *e.g.* the M&DSIG database (Zolensky *et al.* 1995; see McDonnell *et al.* 1997 for details) and is shown as a curve with error bars representing the typical spread in the data. The isotropic model fits (dashed curves) are shown in comparison.

shot program was undertaken using the University of Kent's 2-stage light gas gun.

3.1 Hypervelocity impact testing of tethers

7 shots were performed; 5 on Spectra 1000 0.75 mm tether, and 2 on 1 mm space-grade aluminium wire. All shots were ~5 km s^{-1}, and the projectiles were glass spheres fired in a 'buck-shot' arrangement (see Taylor *et al.* 1997) at a 2×2 cm target area holding 9 strands of tether (all but one target held under a few tens of Newtons tension) or aluminium wire. Typically, about a dozen impactors reached the target area. This data set is also compared to that of Sabath (1996) which comprised of 16 shots on 3 tether types using a plasma drag accelerator; projectiles 20–100μm glass beads, at velocities 3–15 km s^{-1}. It should be noted that none of the impacts

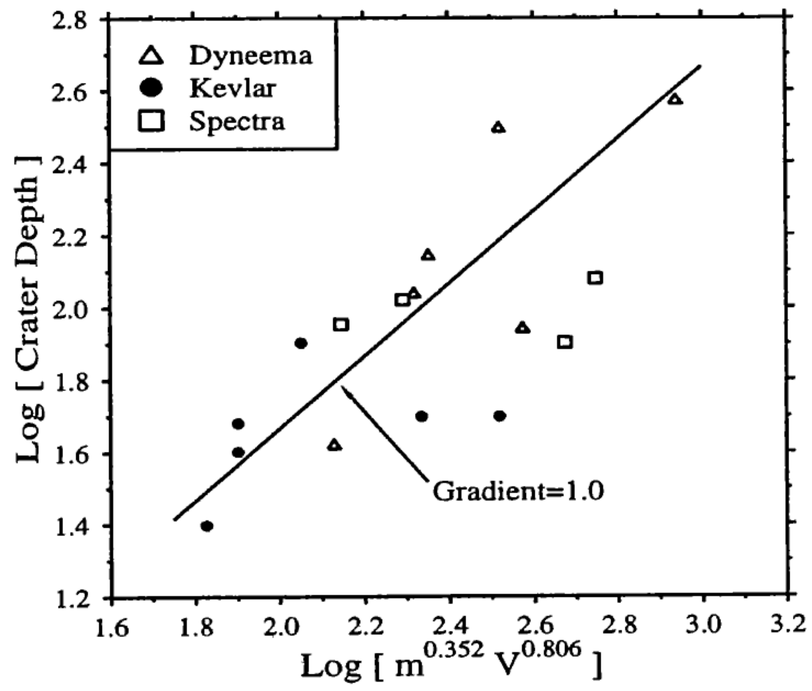

Figure 5: Data from Sabath (1996) used to test the $m^a V^b$ scaling used in Eq. 2 when applied to typical tether material. Although scattered, a general linear trend is observed.

in Sabath's program was sufficient to sever any of the target tethers (failure analysis was performed by energy scaling).

3.2 Wire cross section effects

Fig. 3a shows a 1 mm aluminium wire impacted with a 300 μm glass sphere (the impact site has been revolved by 90° for clarity). We see that the crater walls have collapsed and the 'hole' cross-section is elongated, resulting in an enhanced penetration depth compared with a foil. We find that in cases of a wire rather than foil cross section, the Eq. 2 under-predicts somewhat, such that

$$F_{max}(\text{actual}) \approx 1.25 F_{max}(\text{from Eq. 2}) \qquad (3)$$

3.3 Impact damage equation for tethers

Now consider whether this 'modified' form of Eq. 2 can adequately predict the impact response of the tether, rather than the more commonly used (and well-tested) metals. Using appropriate constants for Spectra 1000 (ρ = 970 kg m^{-3}, σ = 2990 MPa), in Eq. 2 (and the modification of Eq. 3) we would predict, for a 5 km s^{-1} impact, and a 300 μm glass projectile, F_{max}~820 μm. This would obviously break the 750 μm diameter tether. Fig. 3b shows the effect of a 300 μm projectile at 5 km s^{-1} and indeed the tether strand is destroyed. However, a 200 μm glass projectile, at 5 km s^{-1} yields a predicted F_{max}~530 μm. This would damage the 750 μm tether, but may not sever it completely. Fig. 3d shows the effect of a 200 μm projectile at 5 km

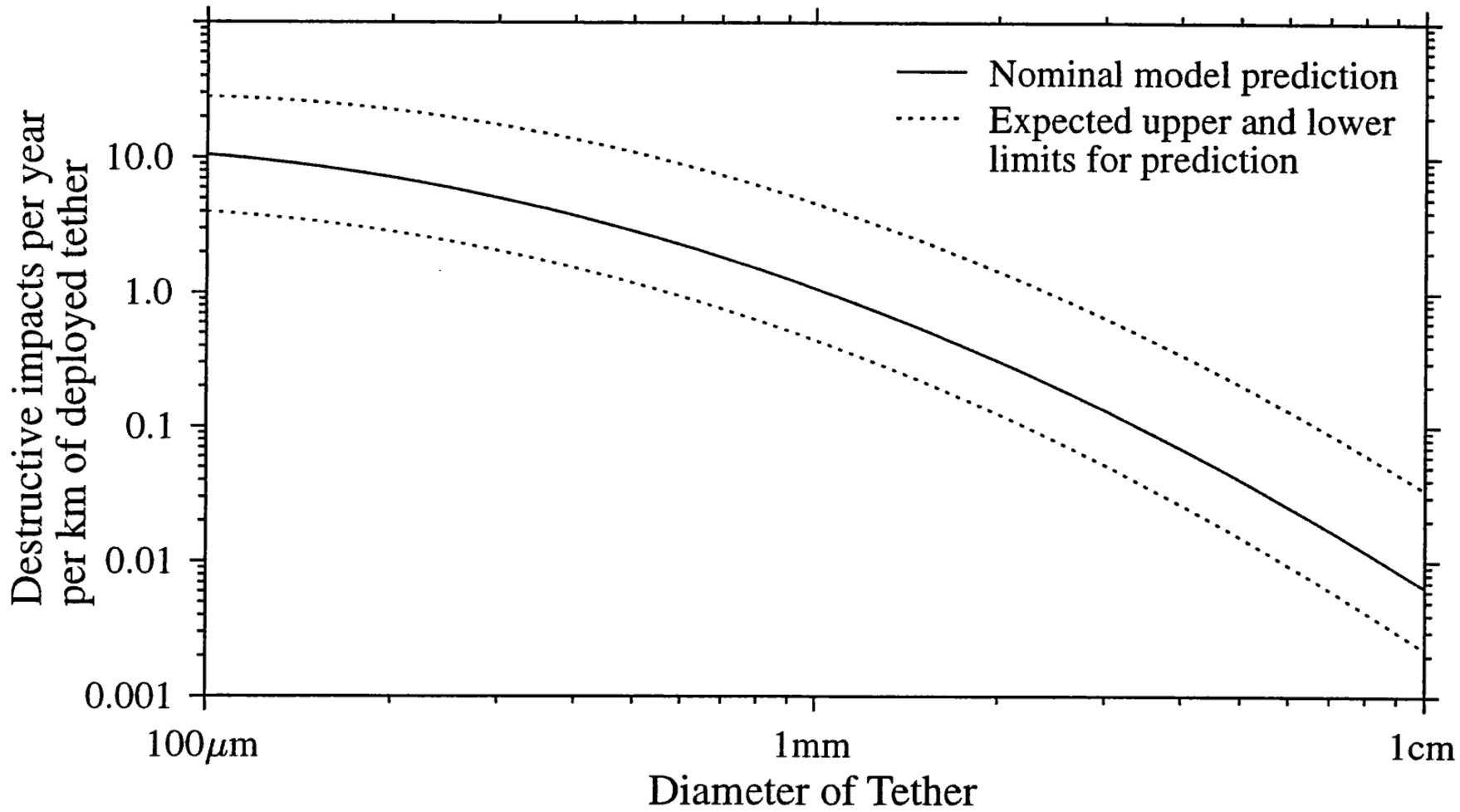

Figure 6: The number N of destructive impacts per year per km of deployed tether. The results apply to a circular cross section tether of a given diameter. The dotted lines give an indication of likely upper and lower limits (see text). A lifetime is calculated by $1/(N \times L)$ where L is the length (km) of the deployed tether.

s^{-1} and indeed the tether strand is damaged but not destroyed. It is not certain that the impact was directly on the tether (as opposed to grazing) although the witness plate positioned behind the target does not show much damage suggesting the projectile was totally disrupted *i.e.* the projectile probably hit essentially centrally on the tether.

We conclude that Eqs. 2 and 3 do adequately predict the tether response at 5 km s^{-1}. We adopt the failure criterion of tethers as being when $F_{max} > D$ where D is the tether diameter (a lower limit based on the data would be $F_{max} > 0.75D$). We can briefly investigate whether the velocity scaling (or 'energy scaling') in Eq. 2 holds (at least to 15 km s^{-1}) by using the data set from Sabath (1996) and using his crater depth as an analogue to our F_{max}. If the scaling holds, we thus would expect a linear relationship between crater depth and $m^{0.352}V^{0.806}$. Fig. 5 shows the Sabath (1996) data set, and a gradient of 1 shown. Although the data are quite scattered, a general linear trend is seen and so we will assume the scaling holds.

3.4 Target area effects

An additional consideration in the model, is that of grazing impacts *i.e.* a potentially destructive impact ($F_{max} > D$) might not sever the tether if the impact is grazing. This is shown in Fig. 3d where a 300 μm, 5 km s^{-1} impactor (*i.e.* potentially destructive) has taken a 'bite' out of a loosely held tether strand in what was obviously a grazing impact. To broadly account for this effect, we shall adopt a criterion that potentially destructive impacts will cause the tether to fail if the projected meteoroid trajectory passes within $R/2$ of the tether centre (where R is the tether radius) *i.e.* 50% of potentially destructive impacts will sever the tether.

4. MODEL RESULTS

Finally we can now run the model for a LEO tether (specifically a 0.75 mm Spectra 1000 strand at 350 km altitude, although generally applicable to typical materials such as Dyneema or Kevlar strands) and consider the rate of destructive impacts as a function of the tether's area-time product. The model is run as a multi-sided LDEF-like cylinder to determine a mean flux to the sides of the structure, with the area exposed being πD per unit length of tether. The model results are shown in Fig. 6, plotted as the number N of destructive impacts per year per km of deployed tether, as a function of the tether diameter D. A parametric fit of this curve gives the form

$$y = a + bx + cx^2 \tag{4}$$

where $y = \log_{10} N$ and $x = \log_{10} D(\mu\text{m})$, and a,

b and c are constants; $a = -0.710$, $b = 2.102$ and $c = -0.618$. Upper and lower limits can be obtained by considering our assumptions. A reasonable upper limit for N is obtained if we assume that the tether failure occurred at our experimentally determined lower limit $F_{max} > 0.75D$, and that *all* the potentially destructive impacts actually sever the tether. Additionally, a reasonable lower limit for N is obtained if we retain our nominal failure criterion of $F_{max} > D$, but if failure only occurs if the projected meteoroid trajectory passes within $\sim 0.1R$ of the tether centre (where R is the tether radius) *i.e.* 20% of potentially destructive impacts will sever the tether. These limits (error estimates) are also shown on Fig. 3, where the curve follows the same fit as in Eq. 4 but with: $a = -1.013$, $b = 2.576$ and $c = -0.626$ (upper dotted curve); $a = -1.521$, $b = 2.404$ and $c = -0.672$ (lower dotted curve).

If we consider the SEDS-2 tether ($\sim$20 km deployed of $\sim$0.75 mm Spectra 1000), using Eq. 4, we deduce a typical lifetime of 11^{+16}_{-8} days. The tether was observed to break in $\sim$4 days. The remaining $\sim$7 km of tether would then have a lifetime of 31^{+45}_{-24} days. The actual tether was observed in orbit, with no obvious severing events for a further $\sim$53 days before the structure began the re-entry process (J.A. Carroll, personal communication). Thus the prediction appears wholly consistent with the observed behaviour of the SEDS-2 tether. For the $\sim$2 mm, 4km TiPS tether (launched June 1996) the predicted lifetime is 295^{+440}_{-230} days. At time of writing, the TiPS tether has been in orbit for $\sim$300 days without breaking.

5. CONCLUSIONS

It is seen that lifetimes of long, thin (< 1 mm diameter) single strand tethers are generally short, making them inappropriate for long duration missions. Multi-strand tethers, or ribbon-like geometries will greatly enhance the overall lifetime of a long tether structure, and this should be considered in future mission planning.

6. ACKNOWLEDGEMENTS

We would like to thank D. Sabath and S. Pavelitz for supplying tether samples for our HVI testing (and D. Sabath also for supplying a copy of his thesis), and J.A. Carroll and M. Kruijff for their useful comments.

7. REFERENCES

Grün, E., Zook, H.A., Fechtig, H. & Giese, R.H., Collisional balance of the meteoritic complex, *Icarus*, **62**, 244-272, 1985.

McBride, N., Taylor, A.D., Green, S.F. & McDonnell, J.A.M., Asymmetries in the natural meteoroid population as sampled by LDEF, *Planet. Space Sci.*, **43**, 757–764, 1995.

McDonnell, J.A.M., Ratcliff, P.R., Green, S.F. & McBride, N., Micro-particle populations at LEO altitudes: recent spacecraft measurements, *Icarus*, in press, 1997.

Sabath, D., Chancen und Probleme des seilunterstützten Wiedereintritts, Ph.D. Thesis, University of Munich, 1996.

Sekanina, Z. & Southworth, R.B., Physical and dynamical studies of meteors: meteor fragmentation and stream distribution studies, NASA contractor report CR 2615, Smithsonian Institution, Cambridge, MA, 1975.

Southworth, R.B. & Sekanina, Z., Physical and dynamical studies of meteors, NASA contractor report CR 2316, Smithsonian Institution, Cambridge, MA, 1973.

Taylor, A.D., The Harvard Radio Meteor Project meteor velocity distribution reappraised, *Icarus*, **116**, 154–158, 1995a.

Taylor, A.D., Earth encounter velocities for interplanetary meteoroids, *Adv. Space Res.*, **17**, 205–209, 1995b.

Taylor, A.D. & McBride, N., A radiant-resolved meteoroid model, this volume, 1997.

Taylor, E.A., Kay, L. & Shrine, N.R.G., Hypervelocity impact on brittle materials: fracture morphology related to projectile diameter, *Adv. in Space Res.*, in press, 1997.

Zolensky, M.E, See, T.H., Bernhard, R.P., Barret, R., Hörz, F., Warren, J.L., Dardano, C. & Leago, K.S., Final activities of the Long Duration Exposure Facility Meteoroid and Debris Special Investigation Group, *Adv. Space Res.*, **16(11)**, 53–65, 1995.